1   Multiconfiguration electromagnetic induction survey for paleochannel internal structure

2   imaging: a case study in the alluvial plain of the river Seine, France.

4   Fayçal Rejiba[1], Cyril Schamper[1], Antoine Chevalier[1], Benoit Deleplancque[2],

5   Gaghik Hovhannissian[3], Julien Thiesson[1] & Pierre Weill[4]

7   [1]*Sorbonne Universités – UPMC Univ Paris 06, CNRS, UMR 7619 METIS, Paris, France*

8   [2]*MINES ParisTech, France*

9   [3] *Centre IRD France Nord– UMR 242, IEES Paris, Bondy, France*

10   [4]*Normandie Univ, UNICAEN, CNRS, Morphodynamique Continentale et Côtière, 14000*

11   *Caen, France*

12   *Corresponding author: Fayçal Rejiba (faycal.rejiba@upmc.fr)*

13   *Running title:* Geophysical Investigations of a Paleochannel

Abstract

The La Bassée floodplain area is a large groundwater reservoir controlling most of the water exchanged between local aquifers and hydrographic networks within the Seine River Basin (France). Preferential flows depend essentially on the heterogeneity of alluvial plain infilling, whose characteristics are strongly influenced by the presence of mud plugs (paleomeander clayey infilling). These mud plugs strongly contrast with the coarse sand material that composes most of the alluvial plain, and can create permeability barriers to groundwater flows. A detailed knowledge of the global and internal geometry of such paleomeanders can thus lead to a comprehensive understanding of the long-term hydrogeological processes of the alluvial plain. A geophysical survey based on the use of electromagnetic induction was performed on a wide paleomeander, situated close to the city of Nogent-sur-Seine in France. In the present study we assess the advantages of combining several spatial offsets, together with both vertical and horizontal dipole orientations (6 apparent conductivities), thereby mapping not only the spatial distribution of the paleomeander derived from LIDAR data, but also its vertical extent and internal variability.

1. Introduction

Dipolar source electromagnetic induction (EMI) techniques are frequently used for critical zone mapping, which can be applied to the delineation of shallow heterogeneities, thereby improving conceptual models used to explain the processes affecting a wide range of sedimentary environments. This mapping technique is very effective for environments in which the spatial structure has strongly contrasted electromagnetic (EM) properties especially that of interpreted electrical conductivity (EC).

Since the seminal work of Rhoades (Rhoades et al., 1976) much research has been conducted to link the petrophysical and hydrodynamic soil properties to the apparent electrical conductivity (EC_a). EC_a is affected by numerous parameters (Friedman, 2005) whose major ones can be separated into three categories: (1) the bulk soil properties (porosity, water content, structure); (2) the type of solid particle (geometry, distribution and cation exchange capacity) mainly related to the clay content; and, (3) environmental factors (EC of water, temperature,…). The clay infilling of paleochannels, and the deposition of alternate layers of conductive (clayey) and resistive (sandy) material in alluvial plain systems, are examples of natural geophysical processes having contrasted EM properties.

EMI measurements have previously been applied to the imaging of conductive fine-grained paleomeander infilling, produced by meander neck cutoff or river avulsion, which can form permeability barriers with complex geometries (e.g. Miall, 1988; Fitterman et al., 1991; Jordan and Prior, 1992; De Smedt at al., 2011). In addition to providing detailed local information on alluvial plain heterogeneities, which can be applied to the study of aquifer-river exchanges (Flipo et al. 2014), the estimation of the geometry of the Seine river paleochannels can provide valuable insight into its paleo-hydrology, as well as physical transformations resulting from climatic fluctuations during the Late Quaternary.

EMI devices are increasingly used for a large number of near-surface geophysical applications, as a consequence of their ability to produce mapping of EC_a over extended areas and at different depths. The main issue of EMI concerns the quantitative mapping of the vertical variations of EC, obtained after multilayer inversion of EC_a, because of the limited number of measurements at different depths (i.e. source-receiver offsets). Despite the spreading use of multiple-frequency and multiple-coil EMI instruments compared to the classic twin coils configuration, a way to overcome this issue is, at least to constrain, and at

66 best to calibrate multilayer inversion of EMI measurements against ERI (electrical resistivity

67 imagery) profiling. A very large body of scientific literature has been published on the study

68 and use of near-surface electromagnetic geophysics, especially in the frequency domain, as

69 described by Everett (2012).

70   By design, an EMI system energizes a transmitter coil with a monochromatic

71 oscillating current, and the oscillating magnetic field produced by this current induces an

72 oscillating voltage response in the receiver coil. The voltage response measured in the

73 absence of any conductive structure is used as a standard reference. However, the magnetic

74 field oscillations are distorted by the presence of nearby conductive structures, such that the

75 voltage signal induced in the receiver coil experiences a shift in amplitude and phase with

76 respect to that observed in the standard reference. This shift can be conveniently represented

77 by a complex number, comprising quadrature (or imaginary) and in-phase (or real)

78 components, which can be interpreted in terms of EC_a (from the quadrature or out-of-phase

79 part) and depth of investigation (DOI) (Huang, 2005). A comprehensive and more detailed

80 description of the EMI principles can be found in (Nabighian, 1988a, 1988b).

81   Although EMI systems were initially used as mapping tools, and were designed to

82 measure the lateral variability of σ associated with a single DOI, the measurements they

83 provide are now generally interpreted to provide information as a function of depth, albeit

84 down to only relatively shallow depths. This interpretation relies on the fact that, for a given

85 soil model, one specific DOI is defined by four device setup parameters: (1) the offset

86 between the transmitter and receiver magnetic dipole; (2) the orientation of the dipole pair; (3)

87 the frequency of the transmitter current oscillations; and, (4) the instrument height above the

88 ground. An EMI survey during which at least one of these parameters is varied can thus be

89 used to resolve depth-related variations of EC. This distribution can be retrieved by solving an

90 inverse problem, which is derived from a large number of applications (e.g. Tabbagh, 1986;

91 Spies, 1989; Nabighian, 1988b; Schamper et al., 2012).

92   The physical model used in the inversion procedure must be suitably adapted to the

93 electromagnetic properties of the surveyed ground. In the case of a medium characterized by

94 typical conductive properties (e.g. low, non-ferromagnetic materials), at a low induction

95 number the quadrature response is interpreted in terms of the apparent ground resistivity,

96 which to a first order approximation varies linearly with the quadrature response (McNeill,

97 1980). In a resistive (EM effects other than induction become non negligible) or highly

98 conductive (low-induction number assumption is no more valid) environment, such as that

99 mapped in the present study, the McNeill equation is no longer valid, and EMI recordings, in

100 particular their in-phase component, must be interpreted within the specific measurement

101 context. One must then take into account, in addition to the EC, the magnetic susceptibility

102 and viscosity, as well as the dielectric permittivity of the local environment, especially if this

103 one is resistive (e.g. Simon et al., 2015, Benech et al., 2016).

104   The present study focuses on the La Bassée alluvial plain, a zone located in the

105 southern part of the Seine basin, 2 km to the west of Nogent-sur-Seine (France). The

106 geophysical campaign has been performed during 3 days of good weather in June during a

107 low water period. The use of geophysical exploration for this investigation is of significant

108 importance, since it should pave the way for the paleo-hydrological reconstruction of the

109 Seine River (estimation of its transversal geometry and paleo-discharge).

110   The aim of this study is to delineate the geometry of a paleochannel (i.e. its thickness

111 and width), using a state-of-the-art 1D inversion routine applied to EMI EC_a measurements.

112 The inverted data consist in a set of EMI measurements implemented with (1) three different

113 offsets, and, (2) for two dipole configurations: horizontal (HCP) and vertical (VCP).

114   Following a description of the study area, we present the technique used to calibrate

115 the EMI measurements, which relies on reference ERI (Electrical Resistivity Imaging)

116 measurements and an auger sounding profile. The EMI inversion is then constrained to limit

117 the solution space to images that are consistent with the observations provided by the ERI and

118 auger soundings. To this end, a local three-layer model is derived with fixed conductivities,

119 and is then introduced into the inversion routine for each position of the surveyed area. The

120 thicknesses of the soil and conductive filling, corresponding to the presumed paleochannel,

121 are determined through the use of an inversion algorithm.

122   **2.   Description of the study area**

123 The study site is located within a portion of the Seine River alluvial plain (locally named

124 "Bassée"), approximately one hundred kilometers upstream of Paris (France), between the

125 confluence of the Seine and Aube rivers to the North-East, and the confluence of the Seine

126 and Yonne rivers to the South-West (Figure 1). This 60 kilometer-long, 4 kilometer-wide

127 alluvial plain constitutes a heterogeneous sedimentary environment, resulting from the

128 development of the Seine River during the Middle and Late Quaternary.

129   Cartographic studies of this area have been carried out in the past, using

130 geomorphological and sedimentological techniques (Mégnien, 1965; Caillol et al., 1977;

131 Mordant, 1992; Berger et al., 1995; Deleplancque, 2016), thus allowing the broad-scale

132 distribution and chronology of the location of the main Middle and Late Quaternary alluvial

133 sheets to be estimated.

134   In addition, the French Geological Survey (BRGM) has compiled a database of more

135   than 500 soundings, which are uniformly distributed over the Bassée alluvial plain, and most

136   of which reached the Cretaceous chalky substrate. A detailed analysis and interpretation of

137   this database has allowed the substratum morphology to be reconstructed, the alluvial infilling

138   thickness to be evaluated, and a preliminary quantitative analysis of the sedimentary facies

139   distribution to be determined (Deleplancque, 2016). The maximum thickness of the alluvial

140   infilling is thus known to lie between 6 and 8 m.

141   Geophysical investigations of gravel pits (after removal of the conductive topsoil)

142   were carried out using ground-penetrating radar (Deleplancque, 2016), and have contributed

143   to the characterization of the sedimentary contrast of the sand bar architecture, between the

144   Weichselian and Holocene deposits. The Weichselian deposits are typical of braided fluvial

145   systems, with fluvial bars of moderate extent (< 50 m) truncated by large erosional surfaces.

146   The thickness of the preserved braid-bars rarely exceeds 1.5 m. The Holocene architecture is

147   associated mainly with single-channel meandering fluvial systems, characterized by thick

148   point-bar deposits (> 4 m) with a lateral extent of several hundred meters, sometimes

149   interrupted by clayey paleochannel infillings. Traces of small sinuous channels, probably

150   using the paths of former Weichseilian braided channels, are also identified at the edge of the

151   alluvial plain.

152   Aerial photography and a LIDAR (laser detection and ranging) topographic survey

153   (Figure 2) have been used to characterize the paleochannel plan-view morphologies (style,

154   width, meander wavelength), of the most recent (Holocene) meandering alluvial sheets in this

155   area (Deleplancque, 2016). These measurements were complemented by auger soundings and

156   [14]C dating of organic debris or bulk sediment (peat), in order to determine a time-frame for

157   the development of the Seine meanders and to allow these changes to be compared with other

158 regional studies (e.g. Antoine et al. 2003; Pastre et al., 2003). The paleochannel investigated

159 in this study is located 2 km to the South-West of Nogent-sur-Seine (covered by a grassy

160 meadow) and is characterized by larger dimensions than the present-day Seine River. Its

161 width is estimated to lie between 150 and 300 m, with a meander wavelength between 2 and

162 3 km. According to the alluvial sheet analysis and the dating of organic material in the mud-

163 plug of the abandoned meander, it is very likely that this paleochannel was active between the

164 Late Glacial and Preoboreal periods (Deleplancque, 2016).

165 **3. Field survey and measurement setup**
166

167 The survey coordinates were determined through the use of a LIDAR map (Deleplancque,

168 2016), combined with the analysis of a series of auger soundings made along a reference

169 transect of almost 400 m in length (Figure 2 and Figure 3). The lateral extent of the meander

170 was delineated using an EMI system (CMD explorer) produced by GF instruments s.r.o., with

171 non-regular gridding and non-perfect overlapping inside the same area.

172 **3.1 ERI and hand auger soundings results**
173   A total of 13 hand auger soundings down to a maximum depth of 2.4 m (Figure 4),

174 were made along the reference profile. Some of these soundings did not reach the base of the

175 paleomeander mud-plug (clay / gravel transition), suggesting that the maximum depth of the

176 paleomeander is greater than 2.4 m. The auger soundings revealed the presence of two main

177 units. The uppermost unit is comprised of topsoil, which overlies a layer of loam containing a

178 significant proportion of gravel and sand in the eastern part of the reference profile. A clayey

179 layer, the bottom of which was not reached in the deepest portion of the paleochannel, is

180 situated below this unit. In some soundings, the clayey facies contains layers of peat (PTA,

181 04, 05, 06, 08, and 09, in Figure 4).

182   The identification of the Holocene clay infilling along this reference profile was

183   confirmed by measuring several and overlapping ERI profiles (24 m common), along the

184   reference transect. For this, a Wenner-Schlumberger array was selected, with 48 electrodes

185   positioned at a 1 m spacing for the first 340 m, and a 0.5 m spacing thereafter.

186   The ERI cross-section (Figure 5) is produced using a dataset of more than 5000

187   measurements. A Wenner-Schlumberger reciprocal array was used, which provides a good

188   compromise between lateral and depth sensitivities (Furman et al, 2003; Dahlin and Zhou,

189   2004).   In order to estimate the interpreted resistivity distribution, the resulting apparent

190   resistivity sections were processed by means of inverse numerical modeling using the

191   Res2dinv software (Loke et al., 2003) with its default damping parameters, and the robust

192   (L1-norm) method. Following a total of 7 iterations, the resulting ERI profiles had an rms

193   error of 0.48% and 0.93%, for the case of the 1 m and 0.5 m electrode spacings, respectively.

194   The resistivity cross-section reveals two main units: an uppermost conductive unit

195   with a resistivity below 20 Ωm, corresponding to a clayey matrix, and a second, more

196   resistive unit with a resistivity greater than 60 Ωm, associated with a medium/coarse-grained

197   silty horizon. The auger soundings are always achieved by a refusal, which is most likely due

198   to the fact that they had reached the resistive second unit. When compared to the analysis

199   achieved using auger soundings, the electrical properties of the topsoil/loam formation appear

200   to be merged with the clayey formation, with the exception of the western portion of the

201   cross-section, which has significant sand and gravel content. This outcome could also be due

202   to the finer spatial resolution of the ERI measurements (electrode spacing of 0.5 m). It is

203   worth noting that the current sensitivity issue associated to the topsoil/loam identification

204   could have probably been overcome with a gradient or a multiple gradient array, without

205   significant loss in DOI (Dahlin and Zhou, 2006).

3.2 EMI surveys and calibration

EMI surveys were carried out using a CMD explorer (GF instruments), at 1-meter height above the ground, with vertical (HCP, horizontal co-planar) and horizontal (VCP, vertical co-planar) magnetic dipole configurations. The CMD explorer operates at 10 kHz, and allows simultaneous measurements to be made with three pairs of Tx-Rx coils (unique Tx coil), using a single orientation (T-mode). Three different offsets were used between the centers of the Tx and the Rx coils, namely, 1.48 m, 2.82 m and 4.49 m, each corresponding to a distinct DOI (approximately 2.2 m, 4.2m, 6.7 m for HCP respectively, and 1.1 m, 2.1 m, 3.3 m for VCP respectively). As the VCP and HCP surveys were made separately in continuous mode (0.6 s time step), slightly different sampling intervals were used. In addition, GPS reception difficulties led to several gaps in the VCP and HCP surveys. It was thus important to carefully evaluate these shortcomings, before merging the HCP and VCP datasets prior to the inversion. As the CMD allows the user to export raw out-of-phase data (including the factory calibration only), no pre-processing is needed to obtain the value of the ratio between the secondary and primary magnetic field amplitude.

Apparent electrical conductivities measured using EMI are particularly sensitive to the orientation of the device, the height above the ground at which the EMI system is setup during the survey, and the 3D variability of the EC. In addition, for the interpretation of the measurements, the ground is assumed to be horizontally layered at any given location, even for the smallest dipole offset. It is worth noting that even if the orientation (vertical or horizontal) and height of the dipole are initialized at the beginning of each survey, variations of orientation and height of the EMI device inevitably occurs and add noise to the measurements.

229   In order to improve absolute (not relative) evaluation of EMI data, in situ calibration

230   of EMI data is important. Ideally, calibration must be performed for several heights and over a

231   perfectly known half space of which electromagnetic properties span over a representative

232   range of EC_a values. For the CMD instrument, calibration factors are provided by the

233   manufacturer for 0 (laid on ground) and 1 m heights. However those factors are valid for a

234   given EC_a range and are dependent on the prospection height (which is never exactly 1 m).

235   This height effect, as mentioned above, has a relative stronger influence on the shortest

236   offsets; consequently, to improve the absolute estimation of EC_a, it is important to have a

237   reference zone where the ground is very well constrained. In order to obtain deeper

238   information than obtained with the hand-made auger soundings, an ERI prospection has been

239   carried out; the inversed ERI section provides reference and absolute values of the local

240   resistivities and can be used in the calibration process as described in Lavoué et al. (2010). It

241   is worth noting that other in situ ways of calibration could be performed (e.g. Delefortrie et

242   al., 2014), particularly, using the theoretical response of a metallic and non-magnetic sphere

243   (Thiesson et al., 2014).

244   During the field data acquisition we faced several difficulties that prevent us to do a

245   CMD profile exactly on the reference profile. Actually, the EMI data used for the calibration

246   have been taken from the mapped data closest to the reference profile. This has led to several

247   positioning and alignment errors because: (1) the EMI data do not exactly cross the reference

248   profile; (2) the EMI data are irregularly spaced along the ERI profile; (3) the orientation of the

249   CMD device was not exactly the same, for each measurement retained for the calibration;

250   and, (4) the height above the surface is changing constantly during the acquisition (less than

251   10-20 cm).

252   In order to compute the EC_a of a layered ground, based on measurements made using a

253   horizontal or vertical magnetic dipole configuration, we used the well-known electromagnetic

254   analytical solution for cylindrical model symmetry, given by (Wannamaker et al., 1984; Ward

255   and Hohmann, 1988; Xiong, 1989). However, in the case of thin layers or high frequency

256   content, convergence problems can be encountered in the numerical integration of the

257   corresponding oscillating Bessel functions. At frequencies below 100 kHz, as in the case of

258   the present study, the numerical filters developed by Guptarsarma and Singh (1997) were

259   found to provide an efficient solution to this problem. The inversion scheme developed by

260   Schamper et al. (2012) was used to invert the EMI measurements. For each offset and dipole

261   orientation, a linear relationship (shifting and scaling) is determined between each measured

262   EC_a and the EC_a estimated from the resistivity models (derived from the ERI panel, Figure 6).

263   Once the calibration is done, the new EMI inversion matches the ERI used for the calibration

264   which illustrates the validity of the procedure. Despite the linear relationship assessed

265   between the EMI and ERI resistivities, several non-linear operations are applied: (1) ERI local

266   1D models along the profile are used to simulate EMI measurements; (2) EMI field data are

267   then fitted (linearly) to those simulations using a non-linear optimization procedure to

268   estimate calibration factors; (3) finally the calibrated/shifted data are inverted with a non-

269   linear forward modeling. Each of the previous operations implies a necessary check to ensure

270   that the calibration process has been correctly applied. Step (3) does not guarantee that

271   estimated interfaces will match the ERT interfaces (1) if the fixed/chosen resistivities are not

272   correct, or (2) if EMI does not integrate the ground in the same way as the ERI in case of

273   strong anisotropy, which seems not to be the case here, since a good match is obtained.

274   The correlation coefficients are comprised between 0.5 and 0.7. Such values can be

275   explained by several sources of errors in the estimation of the EMI apparent conductivities

276   along the reference profile: (1) the differences in the location between the EMI measurements

277   used for the calibration and the ERI profile; (2) the fact that the one dimensional model used

278   for the EMI modeling is extracted from the inversed 2D resistivity section; and, (3) the

279   difference of sensitivity between the ERI and EMI data. The regressions indicate the need of a

280   stronger correction for the VCP configuration than for the HCP configuration. The scaling

281   correction decreases as a function of offset, particularly for the HCP, which can be explained

282   by the fact that small offsets are more sensitive to positioning and orientation errors, as well

283   as to natural near-surface variabilities.

284   **3.3 EMI inversion parameters**

285   Once the calibration process is completed, the corrected, apparent HCP and VCP

286   conductivities are inverted, following their interpolation (by kriging) onto the same regular

287   grid. The ERI results indicate a two-layer model (but do not highlight the topsoil), while the

288   auger sounding show a topsoil layer of a few decimeters thickness above the conductive

289   formation. Consequently, a three-layer model seems reasonably justified all over the site

290   during the inversion process to represent the studied area: a resistive topsoil, a conductive

291   clayey filling, and a resistive sand/gravel layer. The resistivity of each layer corresponds to

292   the peak values of the bimodal histograms of the reference 1-meter-spaced ERI profile, as

293   shown in Figure 7. The topsoil EC derived from the half-meter-spaced ERI profile in the

294   western portion is found to be very similar to the EC of the resistive layer inferred from the

295   1m-spaced ERI profile: thus, the first and third layer EC are considered to be equal. This leads

296   to the following model for the mean EC of the three layers: $\sigma_1 = 13$ mS/m; $\sigma_2 = 72$ mS/m; σ_3

297    $= 13$ mS/m. It should be noted that the CMD explorer is operated at a single frequency (10

298   kHz). The sounding height was taken to be 1 m for all the field measurements.

299   It is worth noting that the 3-layer model chosen instead of a 2-layer model, all over the site,

300   could be questionable. Letting the inversion process decide between a 3 or 2-layer model

301   could have been an option. In the present case, the difference between a 2-layer or 3-layer

302   model is clearly negligible where the interpreted thickness of the topsoil (for the 3- layer

303   model) is less than a few decimeters. For such low thicknesses the topsoil can be considered

304   as non-existent considering the acquisition geometry and settings of the CMD explorer.

305   Figure 8 shows the inverted thicknesses of the first and second layers, and the data residual

306   for the HCP (3 offsets), the VCP (3 offsets), and the combined HCP and VCP conductivities

307   (6 apparent values). The standardized root-mean-squared residual (SRMR) for N independent

308   measurements is given by:

$$SRMR = \sqrt{\frac{\sum_{i=1}^{N}\left(\frac{d(i)-d_{meas}(i)}{std(i)}\right)^2}{N}} \tag{1}$$

309   Where N is the number of data points, d is the forward response of the estimated model at the

310   end of the inversion, d_{meas} contains the data, and std is the standard deviation of the data. The

311   standard deviation std was estimated from repeated measurements at several locations, as

312   1 mS/m (with a minimum error of 5%).

3.4 EMI results

3.4.1 General trend

315   The layer thickness inversion was performed using three different datasets: (1) the HCP

316   dataset, (2) the VCP dataset, and (3) the combined HCP and VCP dataset (Figure 8).

317   Whatever the dataset used for the inversion, the thickness computed for the topsoil

318   formation (indicated by *"Thickness 1"* in Figure 8) is globally very small (blue), whereas that

319   computed for the conductive infilling (indicated by *"Thickness 2"*) has a significantly higher

320 value (red), and *vice versa*. Although it varies in thickness, the conductive layer formation

321 spans most of the survey area, whereas the resistive topsoil formation varies mainly in two

322 distinct locations: (1) the south-western limit of the surveyed area, where it reaches a depth of

323 2 m; and, (2) the mid-northern portion of the surveyed area, where its thickness never exceeds

324 0.6 m. In addition, very small scale topsoil formations are scattered over the surveyed area. In

325 all places where the estimated thickness of the first layer is less than 20 cm, the topsoil can be

326 considered as inexistent and a 2-layered model is enough to explain EMI data. Nevertheless,

327 all of the observed topsoil formations appear to be correlated with a local increase in data

328 residual. The thickness of the conductive infilling lying below the topsoil formation ranges

329 between 0 m, in the south-western portion of the studied zone, and its maximum value of

330 almost 2 m at the center of the map.

331   The VCP mode increases the measured thickness of the shallowest portions of the

332 topsoil layer, whereas the HCP mode tends to negate this layer over most of the surveyed area

333 (central part), where it is not extremely thick. This tendency appears to be correlated with a

334 slight increase in the thickness of the second conductive layer.

335   The inversion of all data, in the form of a single dataset, appears to lead to a mixture of

336 the properties inherent to each of the constituent datasets. This outcome is particularly

337 noticeable in the case of the topsoil formation, where certain structures retrieved by both

338 datasets are emphasized with respect to structures that are present in only one or the other of

339 these.

340 **3.4.2 Internal variability**

341 In addition to strong meander wavelength variations, each dipole orientation reveals different

342 level of heterogeneities in the material present in the conductive infilling, as well as the

343 topsoil. Concerning the material close to the surface (< 2 m), this variability is clearly

344   illustrated by the auger soundings, whereas the conductive unit identified by the ERI section

345   is considerably more complex. In simple terms, the thickness of the conductive material tends

346   to decrease, wherever the silty and sandy material reaches the surface.

347   It should be noted that the inversions observed for each dipole orientation are not

348   systematically preserved in the inversion produced by combining the data from both dipole

349   orientations. This result indicates that in the present context, each orientation is

350   complementary, and contributes a specific set of information. This is particularly relevant in

351   the northern portion of the studied area, where the thickness of the first resistive layer is more

352   variable when it is measured with the horizontal dipole configuration (VCP), than with the

353   HCP configuration.

354   The data residual has numerous peaks in the south-western portion of the study zone.

355   In this zone, the resistive topsoil reaches a thickness of 1 m, leading to EMI measurements

356   with a lower sensitivity (and thus lower signal to noise ratio - SNR). The combined

357   HCP&VCP data inversion naturally leads to the occurrence of higher values of data residual

358   than in the case of the individual HCP or VCP inversions. Indeed, it is difficult to compare the

359   data residual maps between the three proposed datasets (i.e. HCP alone, VCP alone and both)

360   as the physical contribution associated to each dataset inversion results is related to the couple

361   dataset & model used for the inversion. HCP and VCP modes do not integrate the ground in

362   the same way exactly. If the ground within the footprint of the EMI system is a bit far from a

363   tabular model, then the interpretation with local 1D models can be more difficult with both

364   data sets combined than with only one of the two sets analyzed. The difficulty to invert the

365   HCP and VCP datasets jointly also arises from the fact that: (1) the locations of the soundings

366   between the two surveys are not exactly the same as the modes cannot be acquired at the same

367   time; (2) the heights varies differently; and (3) the pitch and roll are not constant. For those

368   last two points one could imagine the monitoring of these "flight" parameters to correct the

369   data, which is routinely done for airborne electromagnetic surveys. But this feature does not

370   exist at the present time for ground based EMI devices.

371   **4. Discussion**
372

373   In the present study, the outcomes of ERI and EMI surveys integrate quite satisfactorily the

374   lithological information provided by the auger soundings, but have not yet been checked with

375   exhaustive hydrological information. During the presented geophysical campaign (low water

376   period), the water level measured from PTA02 to PTA04 and from PTA11 to PTA13

377   locations indicate a groundwater situated at 1 m depth, roughly at the interface between the

378   clay infilling and the upper geological unit (Figure 4). In the survey area the water table could

379   rise close to the surface at high water periods, which implies that the conductivity of the

380   topsoil/loam formation should increase. In the closest piezometer located 1 km west from the

381   prospected site, the water table was situated at 70 cm below the surface. The EC measured in

382   the same piezometer in 2011 was 640 µS/cm (12Ωm) and showed a seasonal variation of the

383   water table of approximately 60 cm (Voies Naviguables de France (VNF) tech. report, 2011).

384   The clay infilling is then always saturated while the topsoil/loam upper unit is almost

385   never dry. Even significant changes in the degree of saturation of the topsoil/loam formation

386   would hardly allow the value of its resistivity to lower down to the resistivity of the clay

387   infilling (~10-20 Ω.m) estimated thanks to the histogram (Figure 7). Consequently, if the

388   thickness of the topsoil/loam formation is significantly larger than a few decimeters, the

389   presence of the water table at the surface does not challenge the three layer model assumption

390   based on the lithological boundaries.

391   From a hydrogeological modeling perspective, one of the most important issues is the

392   assessment of the constitutive relationship that links EMI/ERI electrical

393   conductivity/resistivity to hydrodynamic properties (i.e. the permeability) because of the

394   difficulty to discriminate the bulk conduction from the surface conduction mechanism. In the

395   present case, a sample located at PTA12 and at a depth between 140 and 160 cm, show major

396   peaks of calcite and quartz, significant peaks of illite-montmorillonite, and small peaks of

397   kaolinite. The clayey infilling corresponds to a saturated marl sediment containing 20-30% of

398   clay and 50-60% carbonate. The high amount of carbonate originates from the weathering of

399   the chalky cretaceous limestones that outcrop on the borders of the alluvial plain. As the

400   salinity is low and the clay content significant, the electrical conductivity of the clayey

401   infilling is essentially driven far more by the surface conductivity than by the pore water

402   conductivity. As it is not the case for the first decimeter of topsoil/loam, it could be another

403   argument that reinforces the pertinence of the three layer model assumption for the inversion

404   process.

405   From a more general perspective, EMI calibrated with ERI and auger soundings

406   contributed to a better characterization of the geometry and variability of this paleomeander.

407   The results reveal a complex cross-sectional geometry of the conductive clayey layer,

408   featuring from the south-west to the north-east: (1) a sharp contact to the south-west with a

409   resistive sand and gravel layer; (2) a roughly constant thickness of 2 meters of the conductive

410   layer, extending over more than 200 m; (3) a decrease of the thickness of the conductive layer

411   (~ 0.5 m) related to the raising of the gravely substrate, over a length of ~ 100 m; and, (4) an

412   increase of the conductive layer to the north-east. Unfortunately, the contact of the conductive

413   layer with the resistive layer to the north-east was not captured due to the limited extent of the

414   surveyed area. It is thus difficult to conclude if the paleomeander is restricted between PTA03

415 and PTA10, with a mean depth of 2 m and a width of 250 m, or if the former channel was

416 wider (> 350 m) with shallower part associated to sand/gravel bars. It is also not excluded that

417 several (2 or 3) small channels were active during low water stages within a larger "bankfull

418 channel", producing local incision of the bed. Nevertheless, and compared to the modern

419 Seine river (~ 50 m wide, up to 5 m deep), this paleochannel attributed to the Late

420 Glacial/Preboreal period shows a larger width, and a significantly larger width-to-depth ratio.

421 These differences are attributed to different paleohydrological and paleoclimatic conditions,

422 with larger water discharges, larger and coarser solid fluxes, and less cohesive soils in the

423 absence of developed vegetation.

424 From a hydrogeological perspective, the paleo-meanders of the Late Glacial/Preboreal

425 period are filled with large but relatively thin (2 m) mudplugs compared to the alluvial plain

426 thickness (6 to 8 m), which should produce little impact on the groundwater flow. However,

427 this should be confirmed by numerical modeling. The study should be extended to paleo-

428 meanders attributed to different climatic periods of the Holocene, which present different

429 morphologies and aspect ratios.

430 **5. Conclusion**
431

432 We presented the results of the geophysical investigations of a paleochannel in the Bassée

433 alluvial plain (Seine Basin, France). The location of this paleochannel and its geometry,

434 suggested by a LIDAR campaign, have been accurately mapped using a multi-configuration

435 (various offsets and orientations) electromagnetic induction device.

436 In order to correct the drift and factory calibration issues arising from EMI

437 measurements, a calibration procedure was implemented, based on the use of a linear

438   correction with ERI inversion results and auger soundings. The shifting and scaling of EMI

439   HCP and VCP measurements was made for the three available offsets (1.48, 2.82 and

440   4.49 m), at a frequency of 10 kHz. Six apparent conductivities allowed the inversion of a

441   reliable three-layer model, comprising a conductive filling with an EC equal to 72 mS/m

442   below the topsoil, and a resistive substratum having an EC equal to 13 mS/m. The

443   conductivities of the three-layer model were adjusted using the bimodal histogram distribution

444   of the reference ERI profile. The inverted thicknesses are characterized by a significant

445   internal variability in the conductive filling and the topsoil, associated with the paleochannel

446   geometry.

447   The joint inversion of multi-offset HCP and VCP configurations leads to a very

448   interesting result, in which the internal variability description is considerably enhanced. We

449   believe that multi-configuration EMI geophysical survey carried out at an intermediate scale

450   should provide a great complement to TDR (Time Domain Reflectometry) for a quantitative

451   and physical calibration of remote sensing soil properties and moisture content. Combined

452   multi offset VCP and HCP prospections could significantly improve the accuracy of

453   hydrogeological modeling by potentially providing a hydrogeological picture of the first

454   meters sedimentary setting in terms of lithological distribution; but it would also lead to a

455   substantial increase in survey costs with the instruments currently available on the market.

456

457

458   **6- Data availability**
459   In order to access the data, we kindly ask researchers to contact the corresponding author.

460

7- Acknowledgement

This research was supported by the PIREN Seine research program (2015-2019). We extend

our warm thanks to Christelle Sanchez for her participation in the geophysical survey and to

Laurence LeCallonnec for carrying out the XRD experiment.

8- References

Antoine, P., Coutard, J.-P., Gibbard, P., Hallegouet, B., Lautridou, J.-P., and Ozouf, J.-C.:

The Pleistocene rivers of the English Channel region, Journal of Quaternary Science, 18, 227–

243, 2003.

Benech, C., Lombard, P., Rejiba, F., and Tabbagh, A: Demonstrating the contribution of

dielectric permittivity to the in-phase EMI response of soils: example of an archaeological site

in Bahrain, Near Surface Geophysics, 14(4), 337-344, 2016.

Berger, G., Delpont, G., Dutartre, P., and Desprats, J.-F.: Evolution de l'environnement

paysager de la vallée de la Seine - Cartographie historique et prospectives des explorations

alluvionnaires de la Bassée, French Geological Survey (BRGM) report R 38 726, 39 p., 1995.

Caillol, M., Camart, R., and Frey, C.: Synthèse bibliographique sur la géologie, l'hyrogéologie

et les ressources en matériaux de la région de Nogent-sur-Seine (Aube), French Geological

Survey (BRGM) report 77 SGN 303 BDP, 108 p, 1977.

Dahlin, T. and Zhou, B.: A numerical comparison of 2D resistivity imaging with 10 electrode

arrays, Geophysical prospecting, 52(5), 379-398, 2004.

Dahlin, T. and Zhou, B.:Multiple-gradient array measurements for multichannel 2D resistivity

imaging, Near Surface Geophysics, 4(2), 113-123, 2006

482   Delefortrie, S., De Smedt, P., Saey, T., Van De Vijver, E., and Van Meirvenne, M.: An

483   efficient calibration procedure for correction of drift in EMI survey data, Journal of Applied

484   Geophysics, 110, 115-125, 2014.

485   Deleplancque, B. : Caractérisation des hétérogénéités sédimentaires d'une plaine alluviale :

486   Exemple de l'évolution de la Seine supérieure depuis le dernier maximum glaciaire, PhD

487   Thesis, PSL Research University – Paris, 273 p., 2016.

488   De Smedt, P., Van Meirvenne, M., Meerschman, E., Saey, T., Bats, M., Court-Picon, M., De

489   Reu, J., Zwertvaegher, A., Antrop, M., Bourgeois, J., and De Maeyer, P.: Reconstructing

490   palaeochannel morphology with a mobile multicoil electromagnetic induction sensor,

491   Geomorphology, 130, 136-141, 2011.

492   Everett, M. E.:Theoretical developments in electromagnetic induction geophysics with

493   selected applications in the near surface, Surveys in geophysics, 33(1), 29-63, 2012

494   Fitterman, D.V., Menges, C.M., Al Kamali, A.M., and Jama, F.E.:Electromagnetic mapping

495   of buried paleochannels in eastern Abu Dhabi Emirate, UAE, Geoexploration, 27, 111-133,

496   1991.

497   Flipo, N., Mouhri, A., Labarthe, B., Biancamaria, S., Rivière, A., and Weill, P.: Continental

498   hydrosystem modelling: the concept of nested stream-aquifer interfaces, Hydrology and Earth

499   System Sciences, 18, 3121–3149, 2014

500   Friedman, S. P.: Soil properties influencing apparent electrical conductivity: a

501   review, Computers and electronics in agriculture, 46(1), 45-70, 2005.

502 Furman, A., Ferré, T., and Warrick, A. W.: A sensitivity analysis of electrical resistivity

503 tomography array types using analytical element modeling, Vadose Zone Journal, 2(3), 416-

504 423, 2003.

505 Guptasarma, D. and Singh, B.: New digital linear filters for Hankel J0 and J1 transforms,

506 Geophysical Prospecting, 45(5), 745–762, 1997.

507 Jordan, D.W. and Prior, W.A.: Hierarchical Levels of Heterogeneity in a Mississippi River

508 Meander Belt and Application to Reservoir Systems: Geologic Note, AAPG Bulletin, 76(10),

509 1601-1624, 1992.

510 Huang, H.: Depth of investigation for small broadband electromagnetic sensors, Geophysics,

511 70 (6), G135–G142, 2005

512 Lavoué, F., Van Der Kruk, J., Rings, J., André, F., Moghadas, D., Huisman, J. A., Lambot, S,

513 Weihermüller, L., Vanderborght, J., and Vereecken, H.: Electromagnetic induction calibration

514 using apparent electrical conductivity modelling based on electrical resistivity

515 tomography, Near surface geophysics, 8(6), 553-561, 2010.

516 Loke M.H., Acworth I., and Dahlin T: A comparison of smooth and blocky inversion methods

517 in 2D electrical imaging surveys, Exploration Geophysics, 34, 182–187, 2003

518 Mégnien, F. : Possibilités aquifères des alluvions du val de Seine entre Nogent-sur-Seine et

519 Montereau, incluant la carte géologique et géomorphologique de la Bassée, French Geological

520 Survey (BRGM) report 65-DSGR-A-076, 452 p., 1965.

521 Miall, A.D.: Reservoir Heterogeneities in Fluvial Sandstones: Lessons from Outcrop Studies,

522 AAPG Bulletin, 72(6), 682-697, 1988.

523 Mordant, D. : La Bassée avant l'histoire : archéologie et gravières en Petite-Seine, Association

524 pour la promotion de la recherche archéologique en Ile-de-France, Nemours, 143 p., 1992.

525 Nabighian, M. N. (Ed.): Electromagnetic methods in applied geophysics (Vol. 1), SEG Books,

526 1988a.

527 Nabighian, M. N. (Ed.): Electromagnetic methods in applied geophysics (Vol. 2), SEG Books,

528 1988b.

529 McNeill, J. D.: Electromagnetic terrain conductivity measurement at low induction numbers,

530 Geonics Technical Note TN-6, 1980.

531 Pastre, J.-F., Limondin-Lozouet, N., Leroyer, C., Ponel, P., and Fontugne, M.: River system

532 evolution and environmental changes during the Lateglacial in the Paris Basin (France),

533 Quaternary Science Reviews, 22, 2177–2188, 2003.

534 Rhoades, J. D., Raats, P. A. C., and Prather, R. J.: Effects of liquid-phase electrical

535 conductivity, water content, and surface conductivity on bulk soil electrical conductivity, Soil

536 Science Society of America Journal, 40(5), 651-655, 1976

537 Spies, B. R.: Depth of investigation in electromagnetic sounding methods, Geophysics, 54(7),

538 872-888, 1989.

539 Schamper, C., Rejiba, F., and Guérin, R.: 1D single-site and laterally constrained inversion of

540 multifrequency and multicomponent ground-based electromagnetic induction data —

541 Application to the investigation of a near-surface clayey overburden, Geophysics, 77(4),

542 WB19-WB35, 2012.

543 Simon, F. X., Sarris, A., Thiesson, J., and Tabbagh, A.: Mapping of quadrature magnetic

544 susceptibility/magnetic viscosity of soils by using multi-frequency EMI, Journal of Applied

545 Geophysics, 120, 36-47, 2015.

546 Tabbagh, A.: Applications and advantages of the Slingram electromagnetic method for

547 archaeological prospecting, Geophysics, 51(3), 576-584,1986.

548 Thiesson, J., P. Kessouri, C. Schamper, and Tabbagh A.: About calibration of frequency

549 domain electromagnetic devices used in near surface surveying, Near Surface Geophysics, 12,

550 481–491,2014.

551 VNF (Voies navigables de France), 2011. Etat des lieux de la piézométrie de la petite Seine,

552 Technical Report (in french), 58p.

553 Wannamaker, P. E., Hohmann, G. W., and Sanfilipo, W. A.: Electromagnetic modeling of

554 three-dimensional bodies in layered earths using integral equations, Geophysics, 49, 60–74,

555 doi: 10.1190/1.1441562, 1984.

556 Ward, S. H. and Hohmann, G. W.: Electromagnetic theory for geophysical applications, In

557 Electromagnetic methods in applied geophysics, Vol. 1 : Theory, pp. 131–311. Nabighian,

558 M.N., 1988.

559 Xiong, Z.: Electromagnetic fields of electric dipoles embedded in a stratified anisotropic

560 earth, Geophysics, 54, 1643–1646, doi: 10.1190/1.1442633, 1989.

561

562 **Figures**
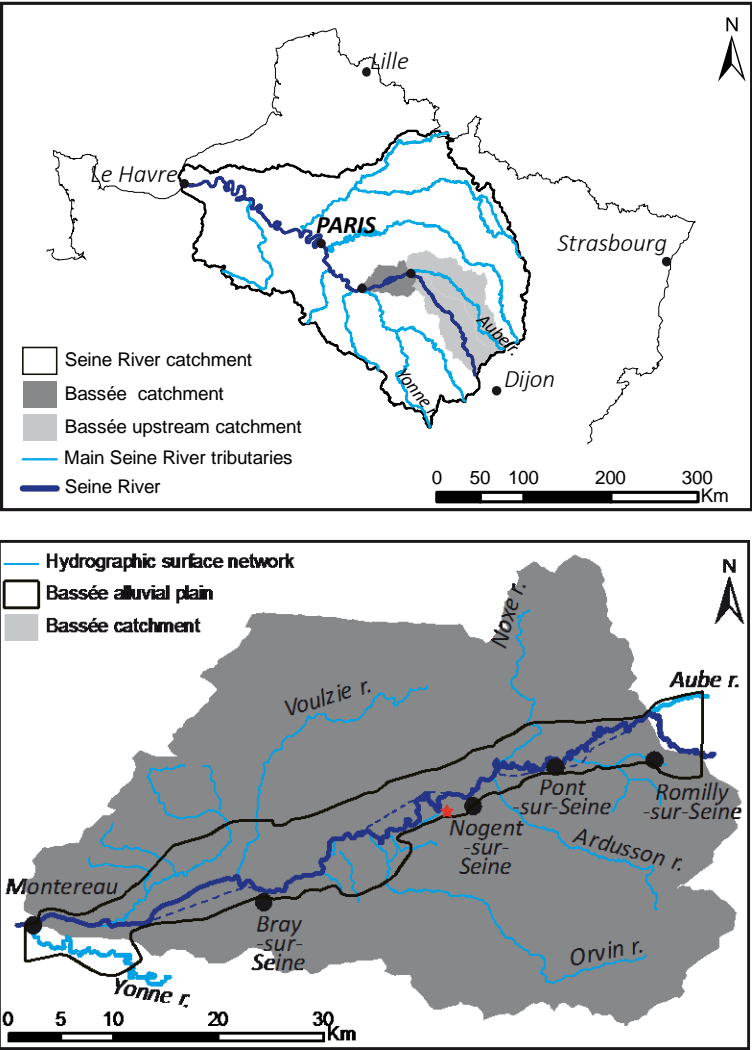
564 Figure 1: Maps of the Seine catchment (top) and the Bassée alluvial plain (bottom).

565

566   Figure 2 : LIDAR map of the study area, showing the contemporary location of the Seine
567   River, together with the narrow and wide paleochannel interpretations.

568

569
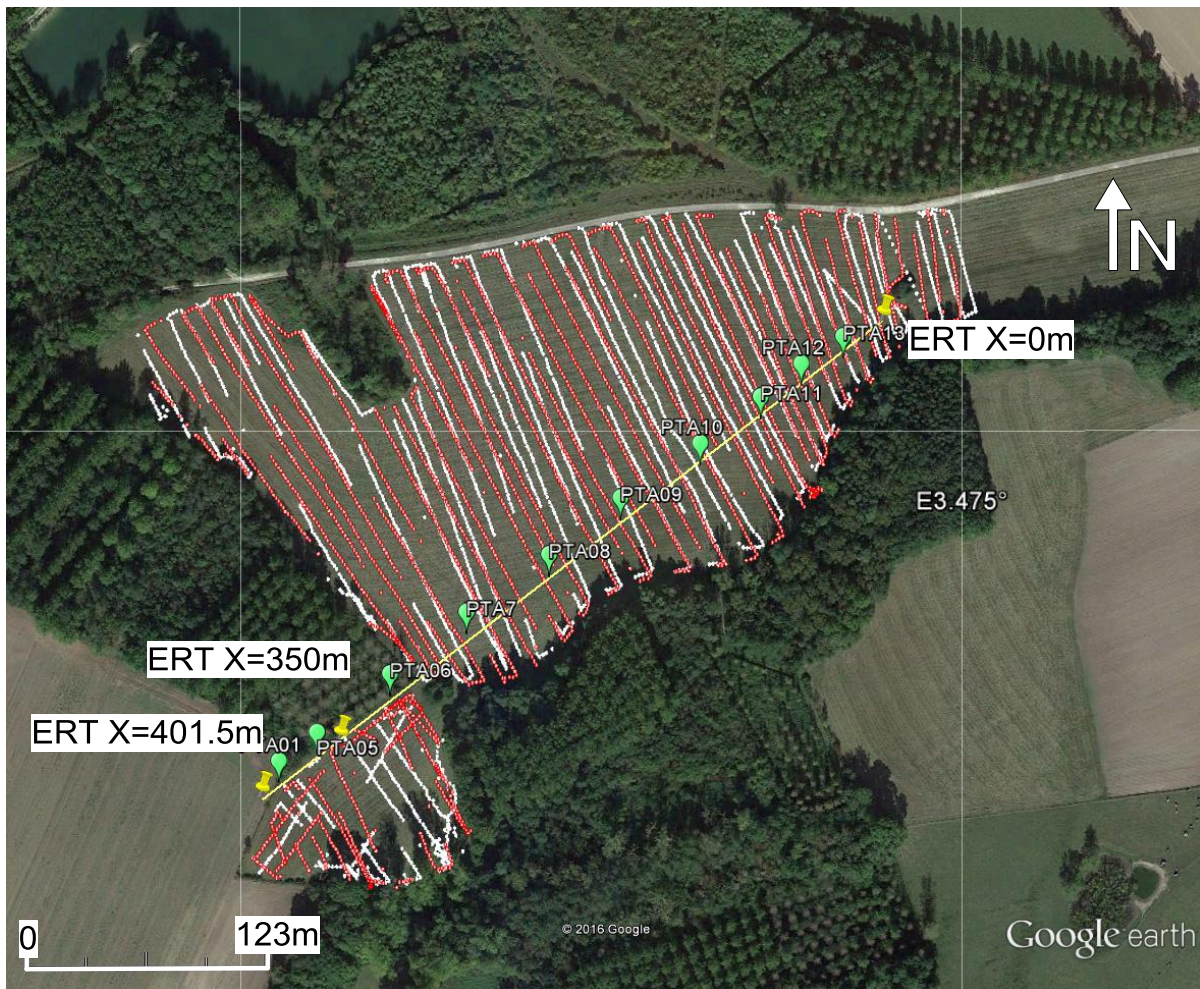
570   Figure 3: Map of the surveyed area, showing the locations of the VCP (red) and HCP (white)

571   measurements (GPS issues explain the holes within the lines). The reference (ERI) profile,

572   recorded with a Wenner-Schlumberger configuration using 1 m electrode spacing between 0

573   and 350 m, and a 0.5 m electrode spacing between 350 m and 401.5 m, is indicated by the

574   yellow line. As green dots, the locations of the hand auger drillings.

575

576
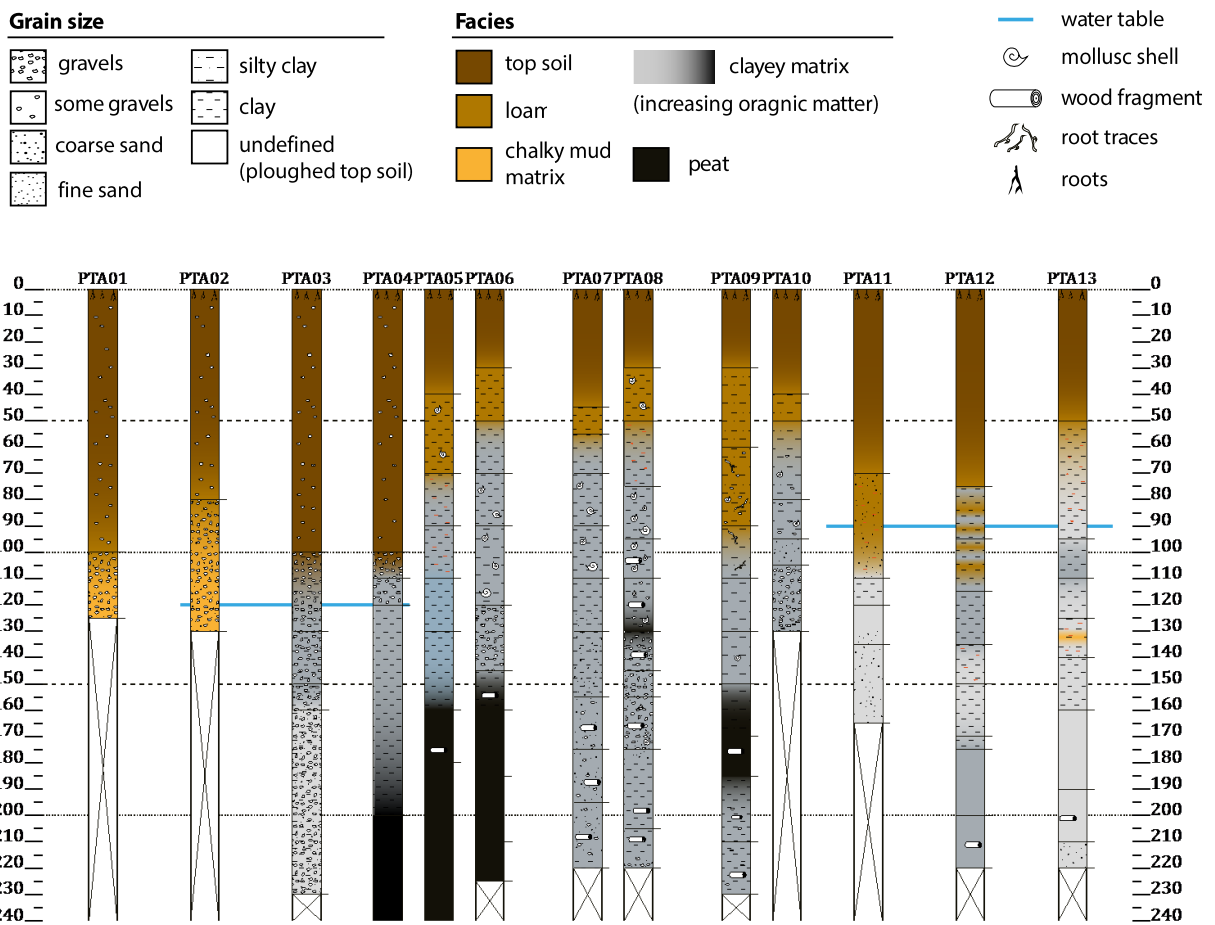
Figure 4: Log of hand auger soundings performed along the reference profile. The position of

each sounding along the ERI profile is shown in Figure 5.

579

580
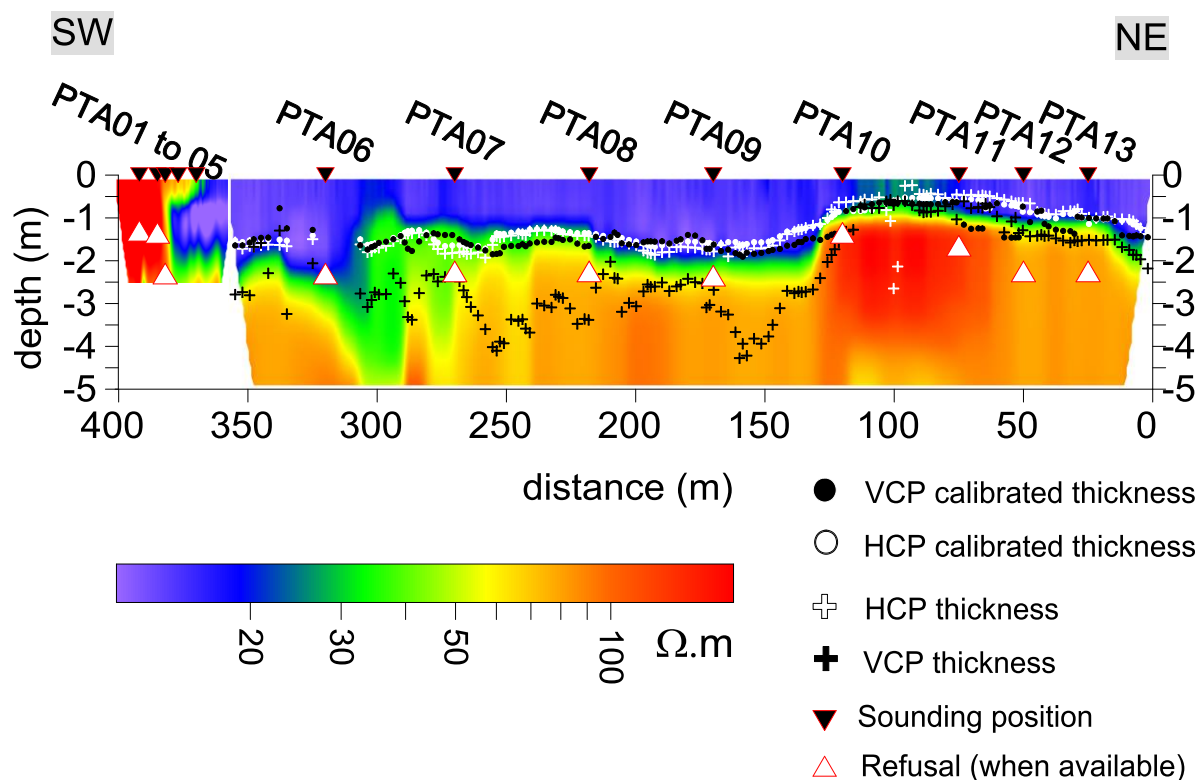
Figure 5: Results from the electrical resistivity tomography (ERI) inversion, computed along

the reference profile. This section reveals the two main (conductive and resistive) geological

units. The markers correspond to the inverted location of the interface (from EMI

measurements) between the conductive unit and the substratum, before and after linear

calibration (Figure 6). This figure shows that calibration of the raw VCP measurements leads

to significant corrections in inverted depth, when compared to the calibration of the HCP

measurements.

588

589
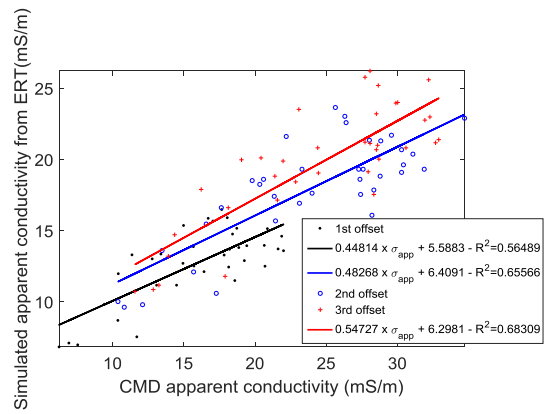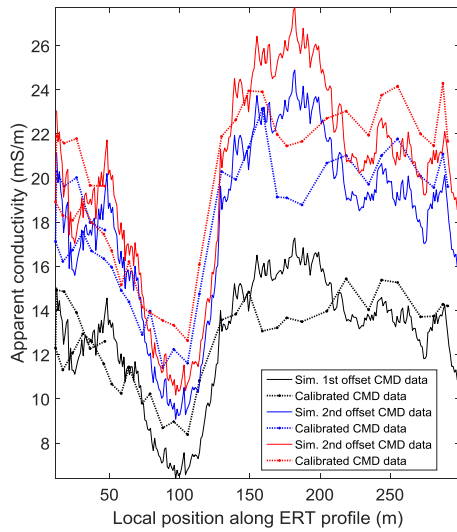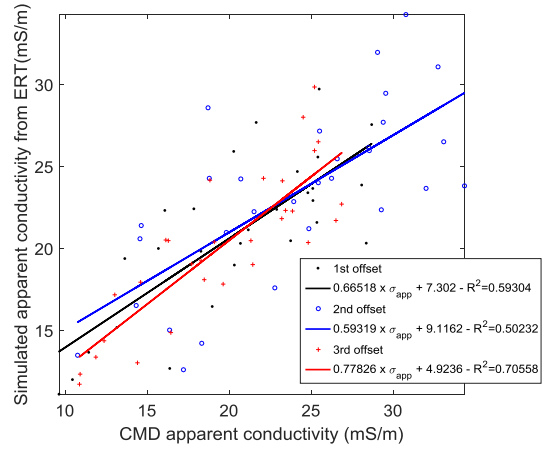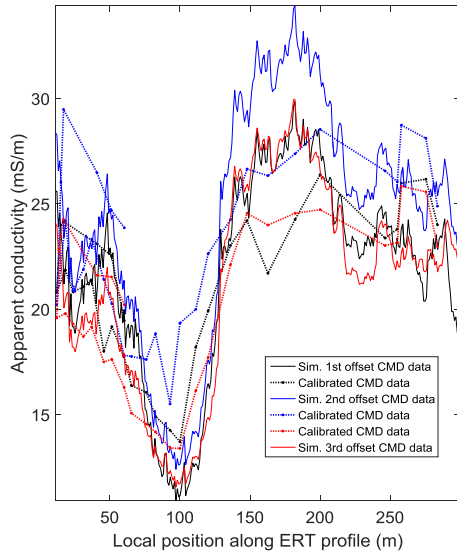
Figure 6: HCP (top) and VCP (bottom) calibration results obtained along the reference profile. Left: the simulated apparent CMD conductivities based on the ERI inversion compared to the calibrated EMI measurements. Right: scatter plots of the measured *vs.* simulated apparent conductivities. The solid lines indicate the corresponding linear regressions.

595
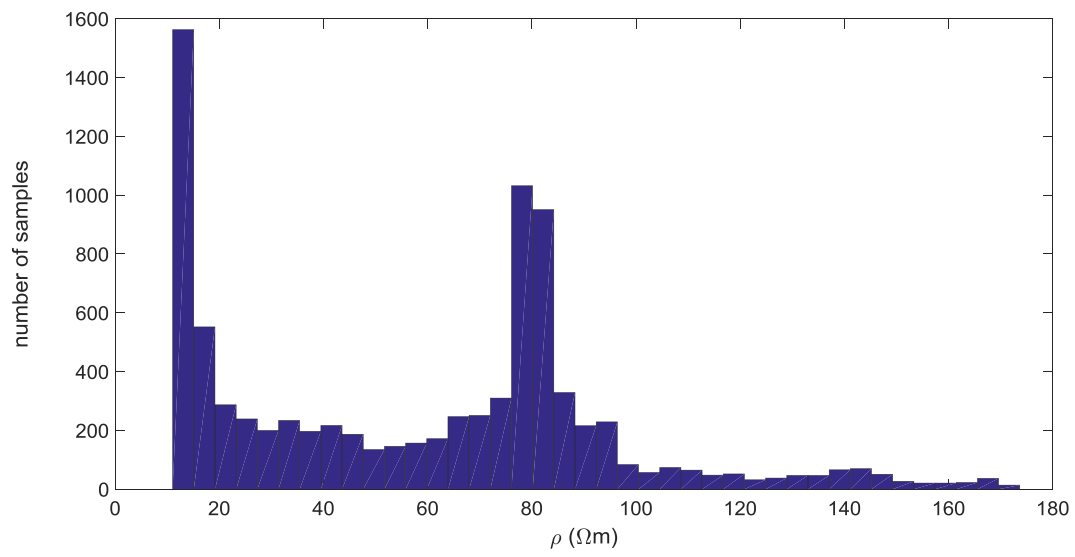
Figure 7: Histogram of the electrical resistivity values determined for the ERI section shown

in Figure 5.

598

599
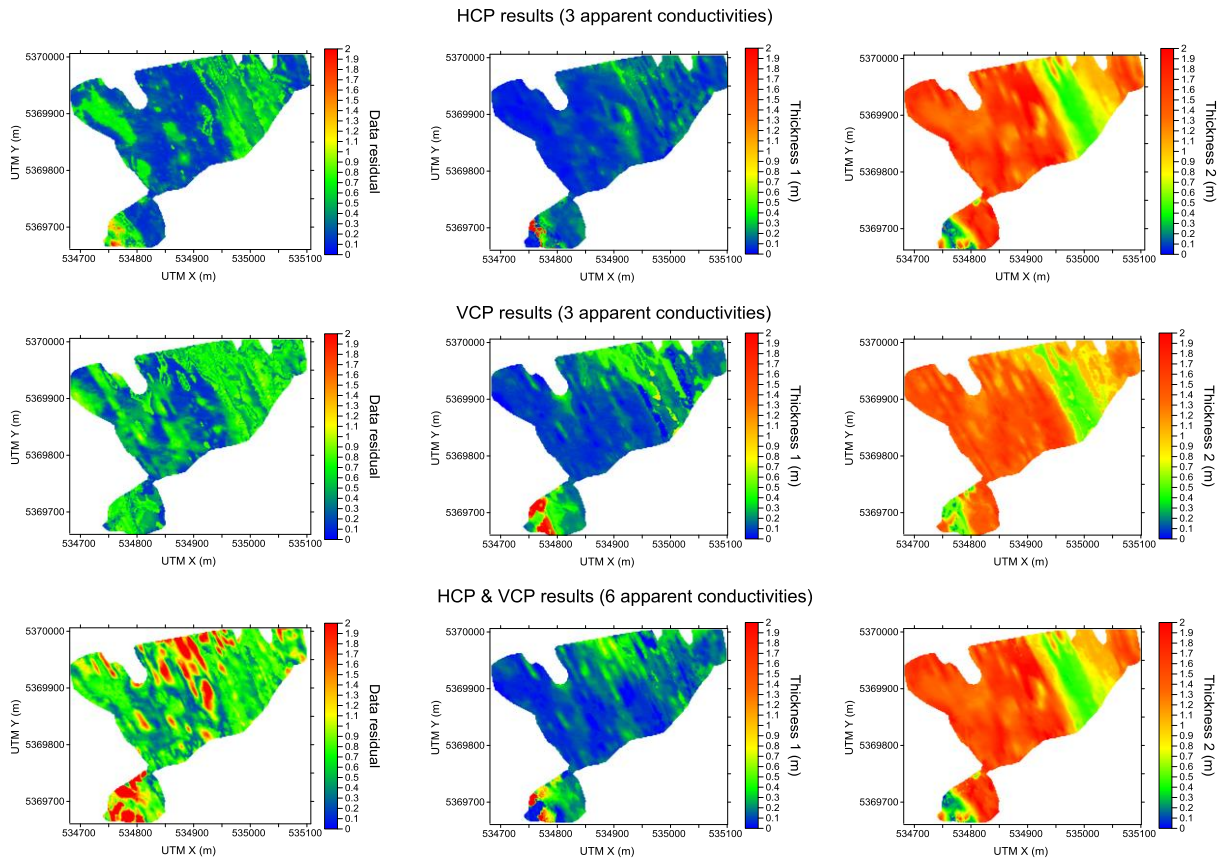
Figure 8: Results of the CMD inversion, including the data residual (left column), for a three-layer model (1: topsoil, 2: conductive filling, and 3: resistive substratum). The thicknesses 1 and 2 correspond to the topsoil and conductive filling, respectively. The prospection height is 1 m. The conductivities are set to $\sigma_1 = 13$ mS/m, $\sigma_2 = 72$ mS/m and $\sigma_3 = 13$ mS/m. A noise level of 1 mS/m on the apparent conductivities was assumed, with a minimum relative error of 5%.

606